

Experimental Considerations of the Chemical Prelithiation Process via Lithium Arene Complex Solutions on the Example of Si-Based Anodes for Lithium-Ion Batteries

Lars Frankenstein, Marvin Mohrhardt, Christoph Peschel, Lukas Stolz, Aurora Gomez-Martin, Tobias Placke, Hyuck Hur, Martin Winter, and Johannes Kasnatscheew*

Losses of Li inventory in lithium-ion batteries lead to losses in capacity and can be compensated by electrode prelithiation before cell assembly or before cell formation. The approach of chemical prelithiation, for example, via Li arene complex (LAC)-based solutions is technically an apparently simple and promising approach. Nevertheless, as shown herein on the example of Si-based anodes and LAC solutions based on 4,4'-dimethylbiphenyl (4,4'-DMBP), several practical challenges need to be considered. Given their reactivity, the LAC solution can not only decompose itself within a range of a few hours, as seen by discoloration and confirmed via mass spectrometry, but can also decompose its solvent and binder of added composite electrodes. Effective prelithiation requires an excess in capacity of the LAC solution (relative to anode capacity) and optimized system characteristic conditions (time, temperature, etc.) as exemplarily shown by comparing Si-based nanoparticles with nanowires. It is worth noting that the prelithiation degree alone does not determine the boost in cycle life, but relevantly depends on previously applied prelithiation conditions (e.g., temperature), as well.

1. Introduction

Lithium-ion battery, the state-of-the-art (SOTA) electrochemical energy storage system,^[1,2] requires further raise in its specific energy and energy density for a successful market penetration of electric vehicles.^[3]

The current development of silicon (Si) as a prominent and advanced (“next-generation”) negative electrode (NE) material is motivated by both, its relative abundance and higher specific/volumetric capacity (3579 mAh g^{-1} , 2194 mAh cm^{-3}) compared to currently SOTA graphite-based NEs (372 mAh g^{-1} , 719 mAh cm^{-3}).^[4–7] However, Si undergoes severe volume changes up to 280% during (de-)lithiation and lowers the cycle life in course of continuous active lithium losses (ALL) (i.e., capacity losses) due to continuous reformation of the passivation layer, the so-called solid–electrolyte interphase (SEI).^[8–10]

Prelithiation has emerged as a highly promising approach to compensate these ALL.^[11,12]


The spectra of prelithiation approaches are wide, among others, including electrochemical prelithiation (sacrificial Li-metal cells, electrochemical bath, electrolysis),^[13–15] prelithiation by physical contact (e.g., Li-metal discs, passivated lithium metal powder (PLMP))^[12,16,17] or chemical prelithiation (e.g., *n*-butyllithium, organolithium complexes like Li-naphthalene, Li-biphenyl (Li-BP)).^[18–20] Given the relative safe handling, control of lithiation degree and homogeneous Li distribution, chemical prelithiation can be a promising strategy from application point of view.^[21,22]

Chemical prelithiation by organolithium complexes are known to pre-lithiate sulfur,^[23] phosphorous^[18] as well as hard carbon.^[24] Solution of 1 M Li-BP in tetrahydrofuran (THF) for example could prelithiate phosphorous/carbon composites according to Wang et al.^[18] claiming stability in ambient air.^[18] However, the redox potential of 0.41 V versus $\text{Li}|\text{Li}^+$ is too high to prelithiate graphite (Gr) or Si.^[18] Jang et al combine biphenyls with dimethoxyethane (DME) showing a stable lithium arene complex (LAC) solution enabling not only the formation of a suitable artificial SEI but also a prelithiation of

L. Frankenstein, C. Peschel, L. Stolz, A. Gomez-Martin, T. Placke, M. Winter, J. Kasnatscheew
MEET Battery Research Center
Institute of Physical Chemistry
University of Münster
Corrensstraße 46, 48149 Münster, Germany
E-mail: johannes.kasnatscheew@wwu.de

M. Mohrhardt, M. Winter
Helmholtz-Institute Münster, IEK-12
Forschungszentrum Jülich GmbH
Corrensstraße 46, 48149 Münster, Germany

H. Hur
Advanced Cell Research Center
LG Energy Solution
Daejeon 34122, South Korea

 The ORCID identification number(s) for the author(s) of this article can be found under <https://doi.org/10.1002/aesr.202300177>.

© 2023 The Authors. Advanced Energy and Sustainability Research published by Wiley-VCH GmbH. This is an open access article under the terms of the Creative Commons Attribution License, which permits use, distribution and reproduction in any medium, provided the original work is properly cited.

DOI: 10.1002/aesr.202300177

Si/SiO_x-based NEs.^[21] Also, by precisely tailored BPs with various electron-donating functional groups, for example, 4,4'-dimethylbiphenyl (4,4'-DMBP), they were able to lower the redox potential and sufficiently prelithiate Si/SiO_x-based NEs.^[21] Shen et al. could even further decrease the redox potential of a LAC solution by exchanging DME either with THF or a strong electron-donating solvent like 2-methyl THF (2-MeTHF).^[25] They were able to suppress cointercalation of 2-MeTHF and even fully lithiate graphite within only three hours.^[25] Worth noting, further lowering the redox potential is redundant as it would additionally raise electrochemical stability concerns, that is, redox potential of 4,4'-DMBP can be regarded as an optimal compromise between sufficient lithiation potential and relative stability.^[18,26]

However, a thorough evaluation from a chemical stability point of view (e.g., of LAC solution itself, solvent, or LAC interaction with composite electrode) of this particular prelithiation technique with these particular chemicals remains uncertain. In this work, chemical stability of solvents (DME, THF, 2-MeTHF) and common binders or binder materials during prelithiation via 4,4'-dimethylbiphenyl (4,4'-DMBP) LAC is thoroughly investigated on their compatibility. With stability-optimized materials, influence of time and temperature is investigated with respect to degrees of prelithiation (DOPL) and its impact on cell performance, which finally is also validated by comparing Si nanoparticles (SiNPs) with Si nanowires (SiNWs).

2. Results and Discussion

2.1. LAC Solution: Stability of Solvent and Binder

The LAC solution is prepared by adding 4,4'-dimethylbiphenyl (4,4'-DMBP) to a Li metal-containing solution according to the scheme in Figure 1a. Within a few hours, the LAC solution decolorizes within initial 8 h, as shown in Figure 1b. This sensitive biphenyl-associated decomposition demonstrates importance of immediate prelithiation after LAC solution preparation.

Solid-phase microextraction–gas chromatography–mass spectrometry (SPME–GC–MS) is applied to investigate stability of an LAC solution at 50 °C, also for dimethoxyethane (DME) and 2-methyl THF (2-MeTHF) solvents, which are frequently used in literature.^[27,28] As chemical and thermal stability are closely intertwined, the elevated temperature is beneficial also to generally conclude chemical stability in a practically more rapid manner. The respective spectrograms ranging from the pristine LAC solution (0 min) to a prelithiation time (*PL-t*) of 8 h are depicted in Figure 2b–d with identical γ -axis. The data indicate decomposition of 4,4'-DMBP for all solvents as seen by the toluene peak at a retention time of ≈ 4.5 min which proceeds in the course of homolytic cleavage of 4,4'-DMBP.^[29] In the DME solvent, some decomposed methylated byproducts are observed. Me radical can stem from radical reaction with DME itself. DME decomposition is further supported by a peak at ≈ 9.5 min retention time. Through a semiquantitative method, the data point qualitatively to a higher stability of THF-based LAC compared

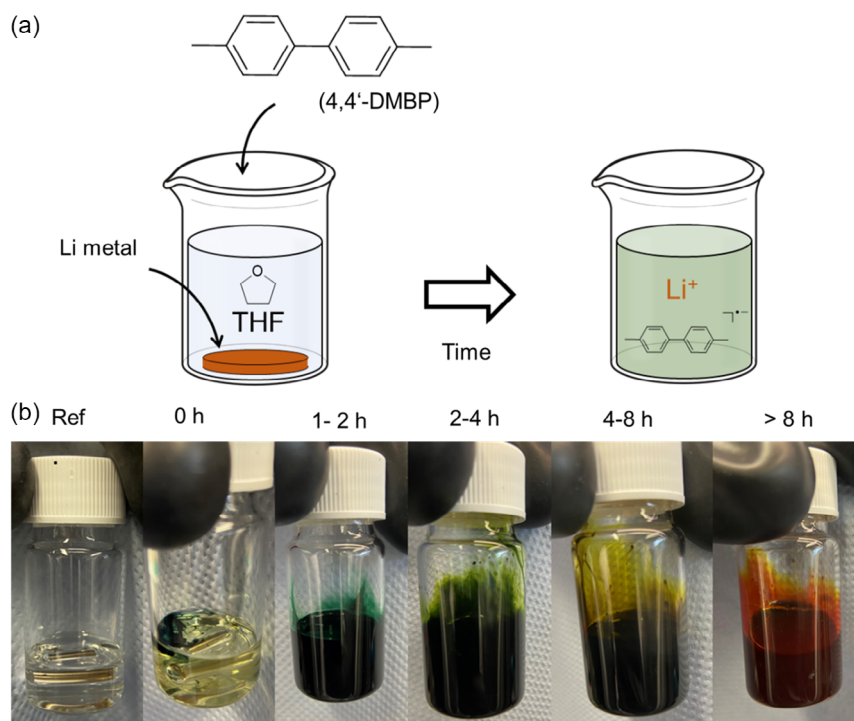


Figure 1. a) Schematic illustration of preparing an LAC solution. Li disc is added to 4,4'-DMBP in THF. b) Images of discoloration during initial 8 h, pointing to chemical reactivity of LACs.

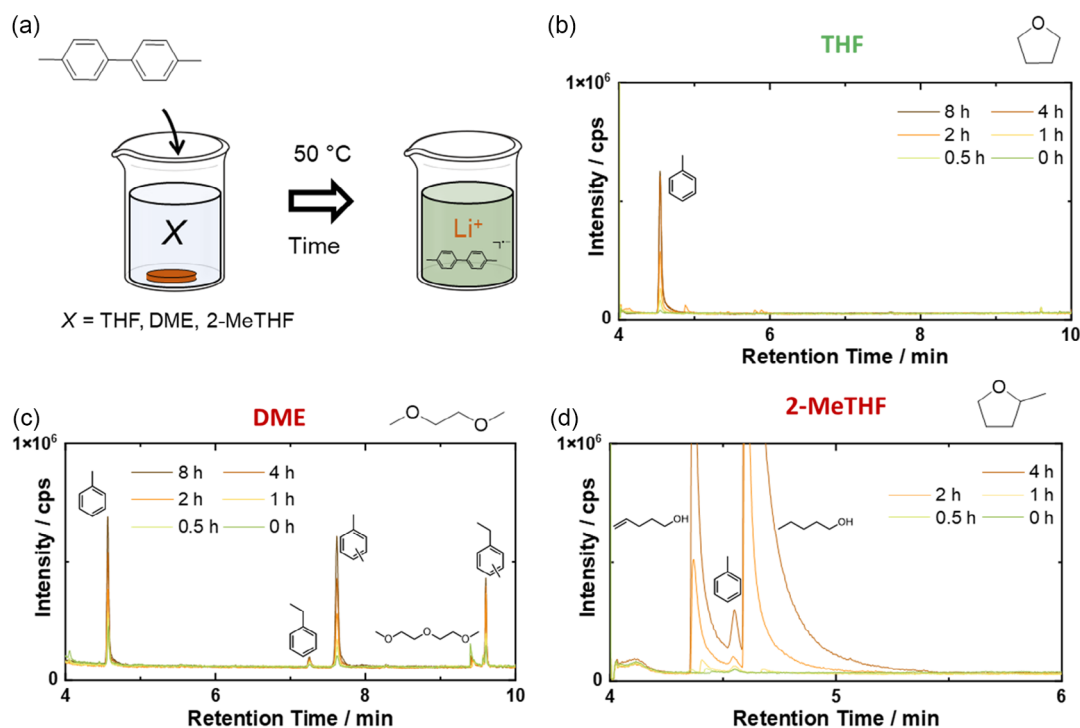


Figure 2. a) Schematic illustration of solvent stability investigation at 50 °C. SPME–GC–MS spectra of b) THF, c) DME, and d) 2-MeTHF. While LAC decomposition products are detectable in all solvents, in line with discoloration observation in Figure 1, only THF is free of additional decomposition products and remains stable.

to DME or 2-MeTHF, which can be also advantageous for direct solvent recycling after pre-lithiation, as discussed in literature.^[30]

During prelithiation of, for example, a SiNW/graphite (SiNW/Gr)-based anode, conventionally composed of a carboxymethyl cellulose and styrene-butadiene rubber (CMC/SBR)-based binder, detachment of the composite from the current collector, is observed as shown in **Figure 3a**, which can be correlated with decomposition of SBR binder, as seen by decomposition via

additional signals (marked in green circles) in ¹H-NMR spectra (Figure 3b).

Possible influence of the binder on the composite detachment in the LAC solution is systematically investigated with ‘model–binder–electrodes’ (binder on current collector only) via Fourier-transform infrared (FTIR) spectroscopy. Here, electrodes are prepared based on SBR, CMC, lithium polyacrylate (LiPAA), and a combination of CMC/LiPAA (7/3 by wt.), being

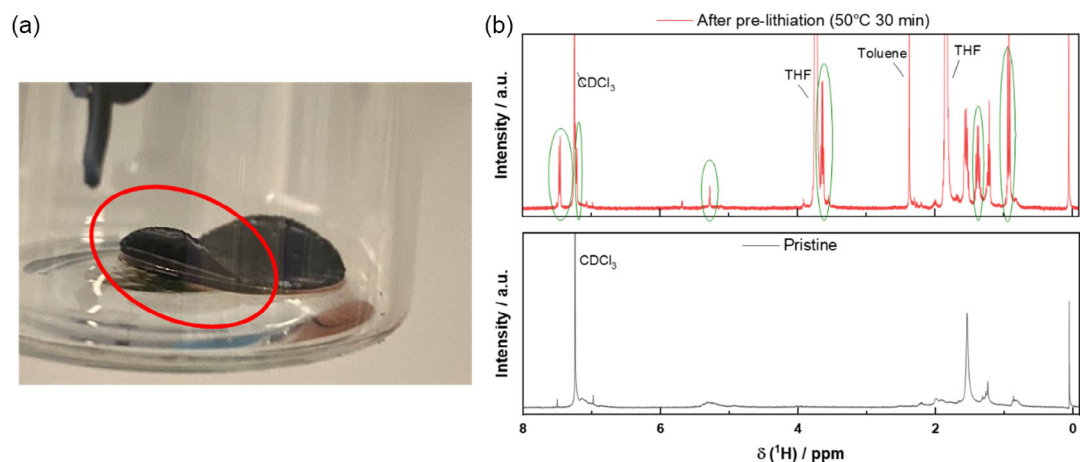


Figure 3. a) Photo of a composite electrode after prelithiation (50 °C, 30 min) showing detachment of the composite from the current collector. b) ¹H-NMR spectra of dissolved SBR binder in CDCl₃ with additional signals pointing to SBR decomposition. Detached composite electrode from current collector can be concluded to be the result of SBR binder decomposition.

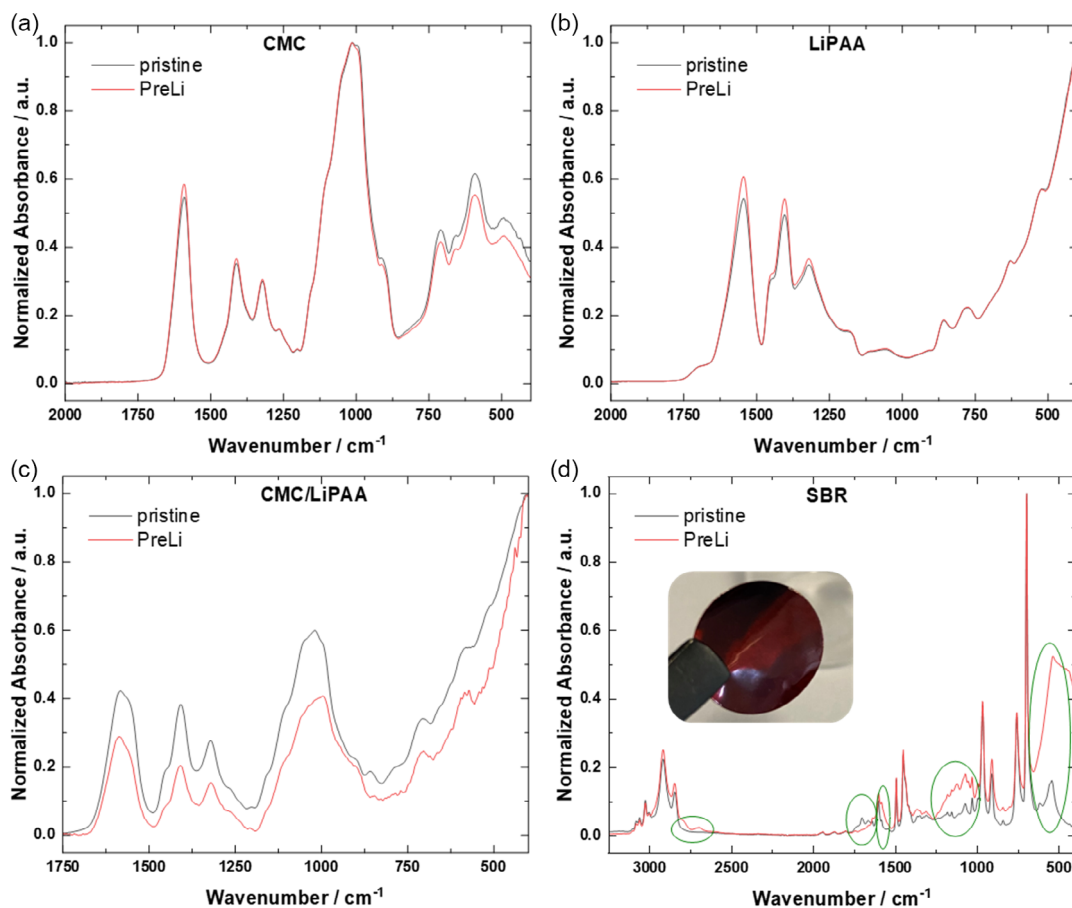


Figure 4. FTIR spectra of pristine (black line) and prelithiated (red line) binder electrodes: a) CMC, b) LiPAA, c) CMC/LiPAA, and d) SBR, demonstrating instability of SBR due to additional signals (marked with green circles).

common binders in silicon graphite (Si/Gr)-based anodes. The measurements are conducted in pristine state and after prelithiation at 50 °C for 30 min, as shown in **Figure 4**. Given the absence of additional signals, CMC and LiPAA indicate stability (Figure 4a–c), while additional signals of SBR (marked with green circles) indicate decomposition, which is also observed via color change.

For validity reasons, the SBR binder is also investigated via ^1H -NMR of SBR (Figure 3b), where the emerged new peaks prove SBR decomposition. SBR instability may consequently be related with the composite detachment (Figure 3) and thus this binder therefore is replaced with LiPAA/CMC (3/7 by wt.)-based binder for further studies.^[31]

2.2. Prelithiation: LAC Capacity Excess, Temperature, and Time

A model electrode consisting of 90% active material (AM) and 10% binder (w/o any conductive additive) is prepared for the mechanistic and validity studies, to, for example, avoid ambiguities in terms of possible lithiation of a conductive agent. This AM consists of SiNP physically mixed with graphite (KS4). For validity reasons, the literature-known application relevant anode based on SiNW is prepared, as well.^[32] The SiNW/Gr. and SiNP/Gr.-based electrodes reveal a first specific delithiation

capacity of 776 mAh g^{-1} and 1485.9 mAh g^{-1} (**Figure 5**), respectively, and serves as reference to determine degree of prelithiation (DOPL) in the next passages and can be regarded as practically maximal specific capacity.

The prelithiation proceeds by putting the anode into the freshly prepared LAC solution according to the scheme in **Figure 6a**. The amount of capacity relative to the capacity of anode plays a decisive role and DOPL increases with increasing LAC amount, that is, rendering LAC capacity excess necessary for an efficient prelithiation, as shown in Figure 6b. However, from an economic point of view, overexcess in LAC capacity is not reasonable as the DOPLs reach a maximum; thus, an LAC capacity excess of 5:1 is sufficient and selected for further investigations.

The DOPL as a function of prelithiation temperature ($PL-T$) is shown in **Figure 7a** and reveals an optimum at 50 °C with DOPL of 60%. The corresponding open-circuit voltage (OCV) values behave vice versa, that is, decrease with $PL-T$ from 0.20 to 0.13 V (from 20 to 50 °C) but show a severe increase to 0.20 V while processing at 60 °C (Figure 7a). Alongside with transfer lithiation effects between graphite and Si,^[33,34] also enhanced LAC- as well as AM decomposition can be speculated to decrease DOPL and increase OCV at 60 °C and render high temperatures not reasonable from DOPL, stability, and energy consuming/cost-efficiency point of view. Powder X-ray diffraction (XRD)

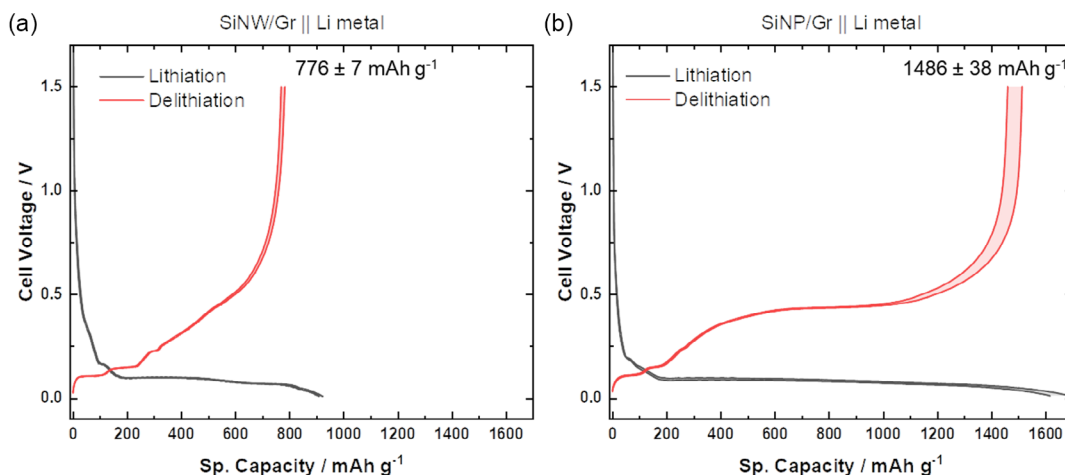


Figure 5. Voltage profiles of initial charge/discharge cycle of a) SiNW/Gr and b) SiNP/Gr-based Li cells, giving practically possible discharge capacities.

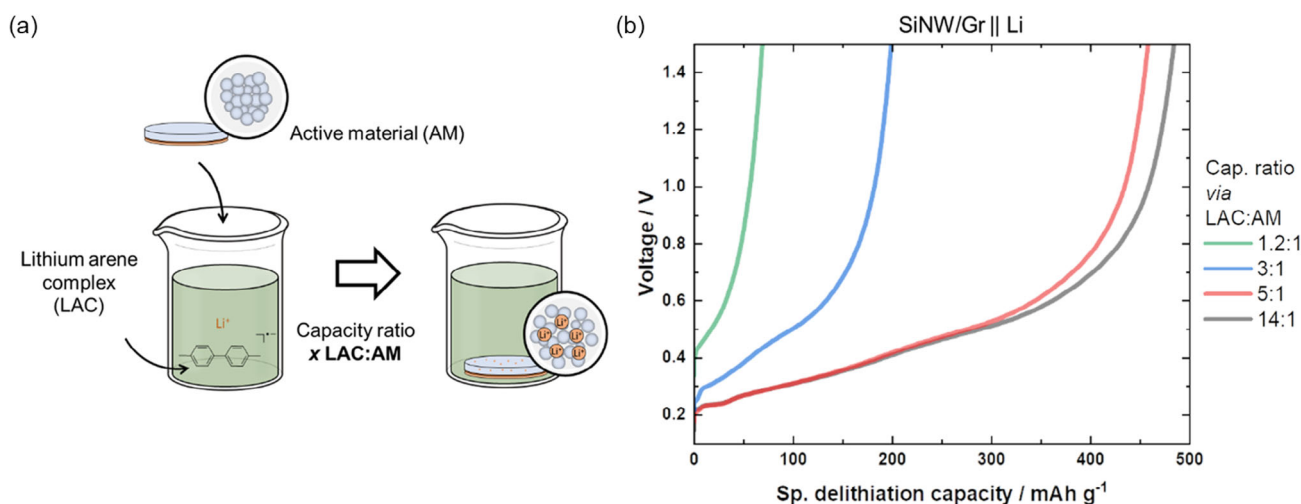


Figure 6. a) Schematic illustration of prelithiation experiment with varied capacity excess of LAC solution relative to active mass of anode, which is achieved via varying 0.5M LAC solution volumes, that is, 0.2 mL, 0.5 mL, 1.0 mL, 2.0 mL for an LAC capacity excess of 1.2:1, 3:1, 5:1, and 14:1, respectively. b) Delithiation profiles after prelithiation (50 °C, 10 min) with varied LAC:AM ratios.

measurements of prelithiated electrodes, shown in Figure 7b, confirm graphite lithiation by both, the LiC_{12} signal and signal disappearance of pure (nonlithiated) graphite. Disappearance of crystalline Si signal after prelithiation also indirectly confirms Si lithiation, as Si gets amorphous when lithiated,^[35] and thus is not detectable via XRD. ^7Li magic angle spinning nuclear magnetic resonance (MAS-NMR) spectroscopy confirms both, lithiated graphite via the LiC_{12} phase at ≈ 42 ppm and lithiated Si (Li_xSi_y), as shown in Figure 7c. Enhanced lithiation in Si with enhanced PL - T can be concluded from peak shift toward lower ppm.^[36] The additional peak at -8 ppm arising at 50 °C can be attributed to a lithiated aryl (Li-Aryl) species.^[37] The existence of this species is also observed via scanning electron microscopy (SEM) and FT-IR measurements of the delithiated electrode (Figure S1a,b, Supporting Information).

The impact of pre-lithiation time (PL - t) is systematically investigated in the range of 20–50 °C (Figure 8). No optimum, instead a temperature-characteristic plateau is observed upon

prolonging PL - t and settles down at a DOPL of 40% (20 °C) and 50% (40, 50 °C) after roughly 2 h. An DOPL optimum is characteristic for each anode type and depends on initial Coulombic efficiency (IC_{Eff}).^[38–41] From an application point of view parameter combination of 40 °C and 10 min can be an economic compromise to achieve relative high DOPLs.^[11,42] Interestingly, besides the characteristically fluctuating OCV and DOPL behavior, the OCV starts to increase after 60 min, though the DOPLs remain relatively constant. Here, a “transfer lithiation” from LiC_x to Li_xSi_y is speculated as well as delithiation processes in course of SEI formation and will be emphasized in future work.

2.3. Full Cell Performance: Degree of Prelithiation Versus Prelithiation Conditions

Prelithiation parameters are validated also for SiNW/Gr-based anodes and shown in Figure 9 in comparison with SiNP-based

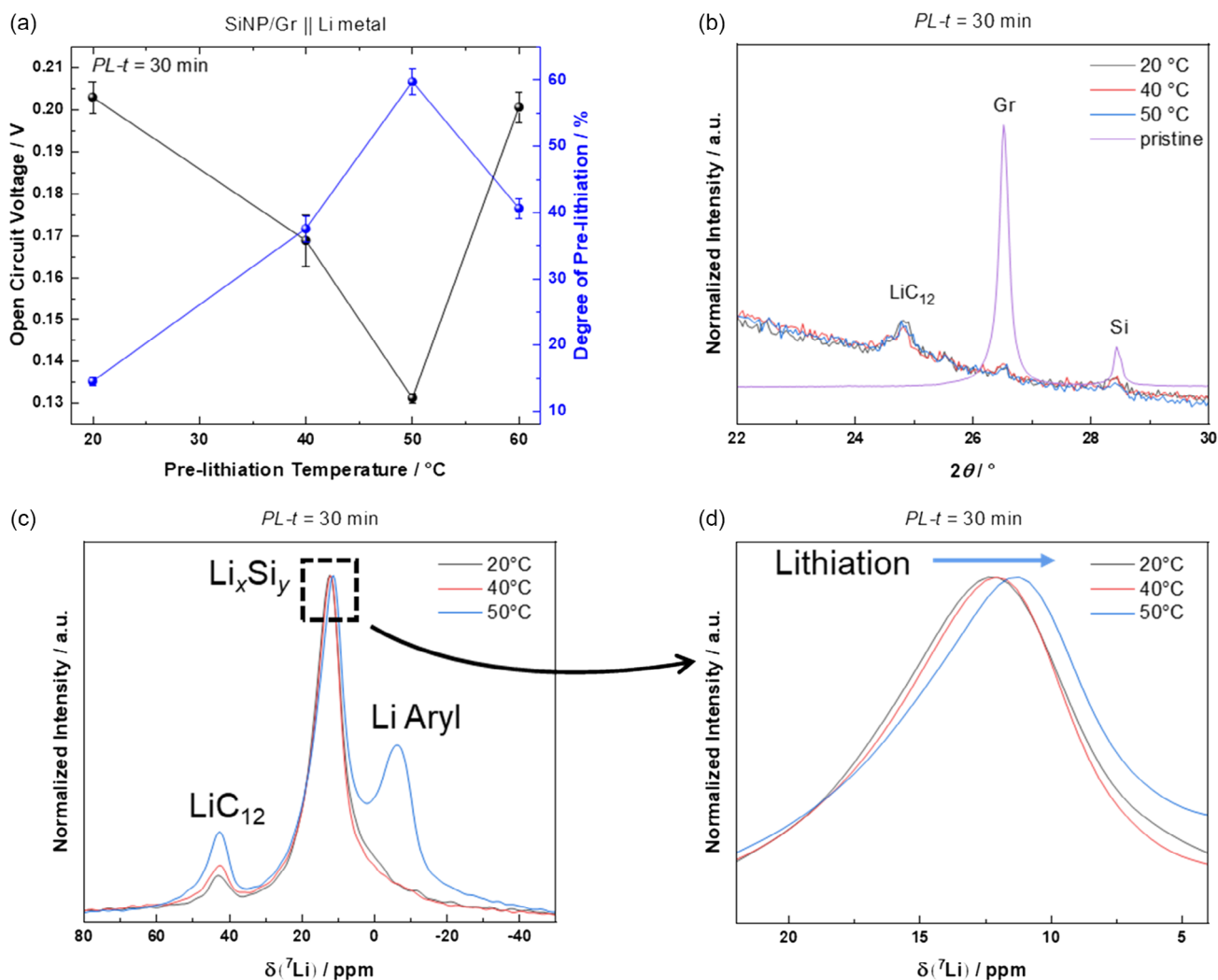


Figure 7. Characterization of prelithiated electrodes after varying temperature for a fixed prelithiation time of 30 min. a) Electrochemically obtained DOPL and OCV of prelithiated electrodes in Li metal coin cells. b) XRD pattern showing partial lithiation in graphite, which is also seen elsewhere. c) ^7Li -MAS-NMR. d) The magnification of ^7Li -MAS-NMR spectra proves also lithiation in the Si-based electrode domain.

anodes, showing anode characteristic DOPLs. Interestingly, the DOPLs have initially higher values starting directly from 45% (20 °C/30 min), which can be related with better lithiation kinetics of thin SiNWs (≈ 18 nm) compared to thicker SiNPs (800 nm),^[43] as well as better Si–Gr contact, as SiNWs are directly grown on graphite as described by Karuppiiah et al.^[44] Improved kinetic aspects of SiNW-based anodes are also observed electrochemically via lower voltage hysteresis (Figure S4, Supporting Information). However, the slight decrease in DOPL at 50 °C/30 min can be related to SiNW degradation. The charge/discharge cycle performance of prelithiated anodes is investigated in $\text{LiNi}_{0.6}\text{Mn}_{0.2}\text{Co}_{0.2}\text{O}_2$ (NMC622)-based cells. As schematically shown in Figure 9b, prelithiation should enhance specific discharge capacity by decreasing capacity loss and indeed is experimentally proven, as shown in Figure 9c. Here, the full cell capacity losses are all similar as they are determined by NMC622 and not by the anode any more. Differences between the differently prelithiated anodes can be observed during

charge/discharge cycling, as shown in Figure 9d. Prelithiation of SiNW/Gr electrodes improves the cycle life for all investigated DOPLs, whereas best combination is achieved for prelithiation parameters of 50 °C/10 min (DOPL of 56%), that is, 173 cycles at 80% state-of-health (SOH), while anodes prelithiated at 50 °C/30 min with similar DOPL reveal only 116 cycles. When pairing higher PL - T with long PL - t , structural damage of not only the binder, but rather the whole composite electrode, can be concluded (Figure S3, Supporting Information), resulting in propagated capacity fading and ALL, rendering harsh conditions (e.g., high temperature) not suitable and DOPL alone not decisive to predict cycle life. It is worth noting that this work focuses on rather extreme conditions (high T , high DOPLs) in order to pragmatically conclude chemical limitations and gain insights into the underlying interplay of parameter, though, in a practically established system significantly, lower DOPLs can be sufficient, which would render the chemical prelithiation relevantly simpler.

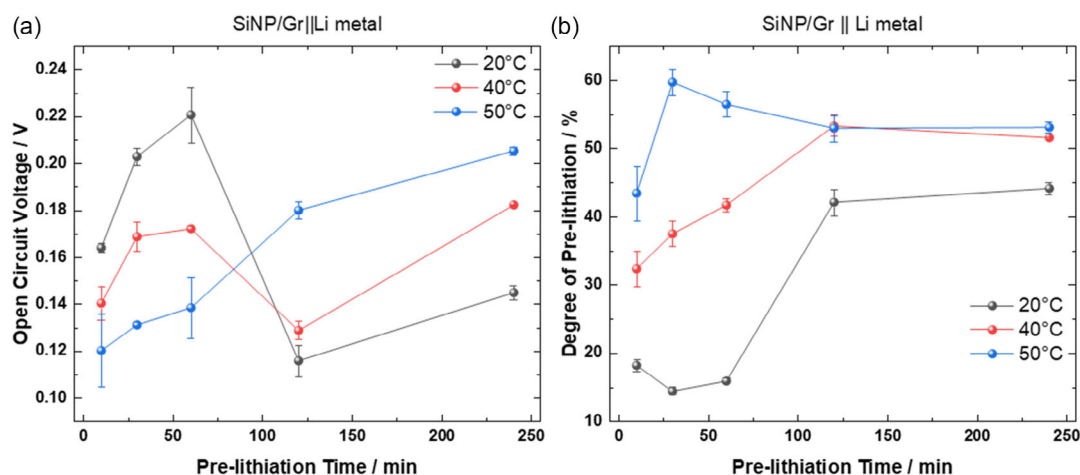


Figure 8. a) Corresponding OCVs for SiNP/Gr-based anodes by variation of PL-t at different temperatures. b) In parallel monitored DOPLs (additional information can be found in Figure S2, Supporting Information).

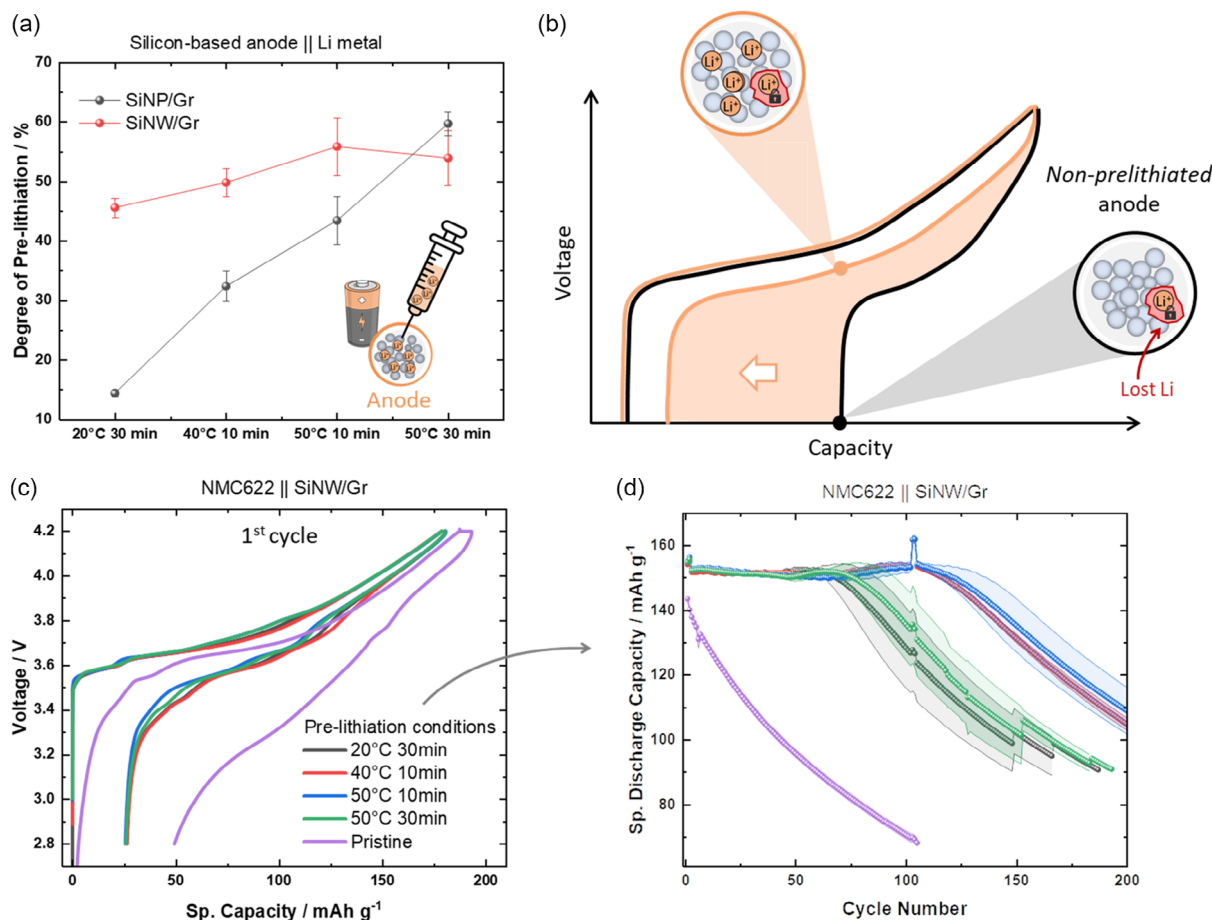


Figure 9. a) Comparing DOPLs at different prelithiation conditions for different Si-based anodes (Si-based nanoparticles vs. nanowires). b) Schematic illustration of the prelithiation influence on the capacity on the example of first charge/discharge cycle voltage profile. c) First¹ charge/discharge cycle voltage profile at 34 mA g⁻¹ (≈ 0.2 C) in the voltage range of 4.2–2.8 V, showing improved specific discharge capacity via decreased capacity loss of prelithiated anodes. d) Specific discharge capacities as a function of cycle number in NMC622 || SiNW/Gr cells showing that DOPL is not the single decisive measure to prolong cycle life. Despite similar DOPLs at 50°C, prelithiation at milder conditions (10 min vs. 30 min) reveals a pronounced higher cycle life.

3. Conclusion and Outlook

Chemical prelithiation, among a variety of prelithiation techniques, is promising for several application-relevant reasons. In this work, prelithiation via a LAC is thoroughly reconsidered on the example of Si-based anodes from practical point of view by selecting 4,4'-dimethylbiphenyl (4,4'-DMBP) as a reasonable compromise in reactivity/lithiation potential (sufficient lithiation of anode at minimized decomposition).

The biphenyls of the LAC solution not only decompose by themselves within a few hours but can also damage prelithiation solution solvents (dimethoxyethane (DME), 2-methyl tetrahydrofuran (2 MeTHF)) and anode binders (SBR), as well. Here, the LAC is shown to be stable with THF and carboxymethyl cellulose/lithium polyacrylate (CMC/LiPAA)-based binders.

To effectively prelithiate the anode, a capacity excess of LAC solution relative to the anode is necessary and is shown to increase the prelithiation capacity of anode from 200 mAh g⁻¹ to 400 mAh g⁻¹, when increasing LAC capacity excess is from 3:1 towards 5:1, while further excess is shown to be less relevant. The prelithiation temperature (*PL-T*) could be shown to have an optimum (here 50 °C), while the prelithiation time (*PL-t*) reaches a plateau. The interplay of *PL-t* and *PL-T* is system (anode) characteristic is demonstrated by comparing SiNWs and SiNPs. It is worth noting that the targeting lower DOPLs via milder conditions (e.g., lower temperature) would minimize any risk of decompositions and the harsher conditions in this work are shown to reveal practical limitations.

The DOPL alone does not directly relate with extension of cycle life, as the prelithiation conditions are decisive, as well. This could be demonstrated by comparing anodes with similar prelithiation degrees, but achieved at different temperatures, which showed pronounced differences in cycle life prolongation, as shown in Figure 10.

4. Experimental Section

Electrode Preparation, Cell Assembly, and Electrochemical Characterization: Composite electrodes with a composition of 90 wt% SiNPs (800 nm) KS4 graphite (SiNP800/KS4) (40 wt%/60 wt%) AM and 7.7 wt% sodium-carboxymethyl cellulose (Na-CMC, Walocel CRT 2000

PPA 12, Dow Wolff Cellulosics) and 2.3 wt% lithium polyacrylate (Li-PAA) (polyacrylic acid (PAA) (M_v ≈ 450 000; Sigma-Aldrich) neutralized with lithium hydroxide (LiOH × H₂O (Sigma-Aldrich))) as binder materials were prepared for systematic model electrode prelithiation. First, Na-CMC and LiPAA binders were stirred in deionized water using a magnetic bar. After complete dispersion, conductive agent as well as the Si/carbonaceous material were added. After addition of each component, the mixture was stirred at 1700 rpm for 15 min for complete homogenization using a planetary centrifugal mixer (THINKY MIXER ARM-310 CE, THINKY CORPORATION). The resulting electrode paste was coated onto smooth copper foil (20 μm in thickness; Schlenk Metallfolien GmbH) using standard doctor-blade technique with a ZUA 2000 Universal Applicator (ZEHNTER GmbH) to ensure the desired coating height and an Automatic Film Applicator 1133 N (Sheen Instruments) with a speed of 50 mm s⁻¹. After electrode processing, the electrode sheets were dried in a laboratory oven (Binder GmbH) at 70 °C for 30 min and electrode discs (Ø = 15 mm) were punched afterward using a Hohsen electrode puncher (Hohen Corp.). Punched electrodes were further dried in a Büchi Glass Oven B-585 (Büchi) at 120 °C for 12 h under reduced pressure (≤ 0.05 mbar) to remove residual water. Afterward, the electrodes were weighed using a Sartorius ME 235S analytical balance (Sartorius AG) with an accuracy of ±0.01 mg and stored at room temperature in a dry room (dew point of at least -50 °C, 0.02% moisture content).

Composite electrodes with a composition of 85 wt% SiNW/Gr (22 wt%/78 wt%) AM, 5 wt% conductive agent (Super C65, Imerys Graphite & Carbon), 7.7 wt% Na-CMC, and 2.3 wt% LiPAA as binder materials were prepared according to the abovementioned preparation technique for investigation of practical full cells.

Model-system binder electrodes for stability investigations were prepared according the same procedure. However, the electrodes contained only the corresponding binder. After drying, CMC, LiPAA, and LiPAA/CMC exfoliated from the current collector, which simplified analysis further. SBR remained as a laminate attached to the current collector.

Electrochemical evaluation of SiNW/Gr electrodes was performed in two-electrode configuration SiNW/Gr || Li metal "half cells" as well as NMC622 || SiNW/Gr full-cells. The Li content of prelithiated SiNP800/KS4 and SiNW/Gr materials was determined by simple delithiation of the electrode versus Li metal applying 75 and 40 mA g⁻¹, respectively (corresponding to 0.05 C). NMC622 || SiNW/Gr cells were cycled 2 cycles at 34 mA g⁻¹ (0.2 C) followed by 100 cycles at 56 mA g⁻¹ (0.33 C) and 2 cycles at 17 mA g⁻¹ (0.1 C), repeatedly. Cell cycling was automatically stopped, when the actual cell capacity reached 60% the capacity of the third cycle.

Synthesis of LAC Solutions: Prelithiation proceeds according Figure 11. LAC solutions were prepared by dissolving 0.5 M 4,4'-DMBP in either dimethoxyethane (DME), tetrahydrofuran (THF), or 2-methyl THF (2Me-THF). After full dissolution of the solid, Li metal (4:1 ratio) was

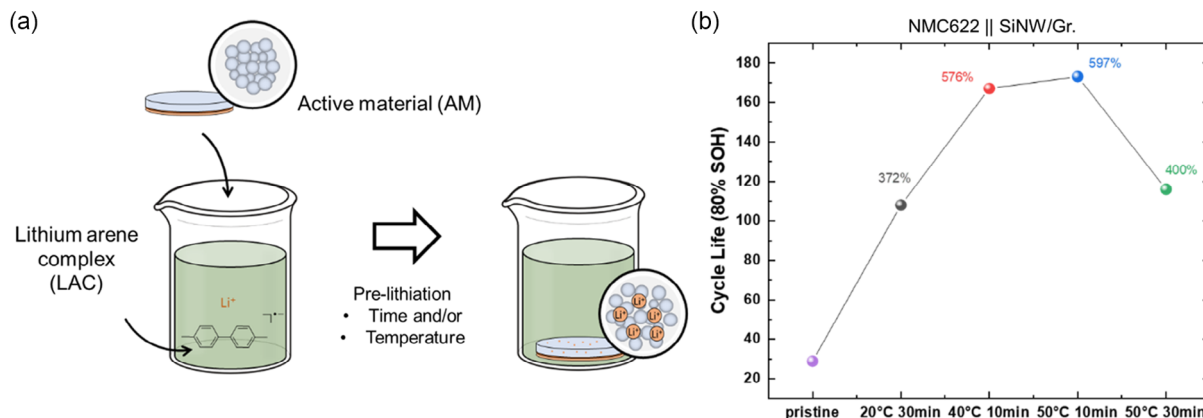


Figure 10. a) Schematic summary of the prelithiation approach using varied processing conditions. b) Cycle number at 80% SOH for varied prelithiation processing conditions.

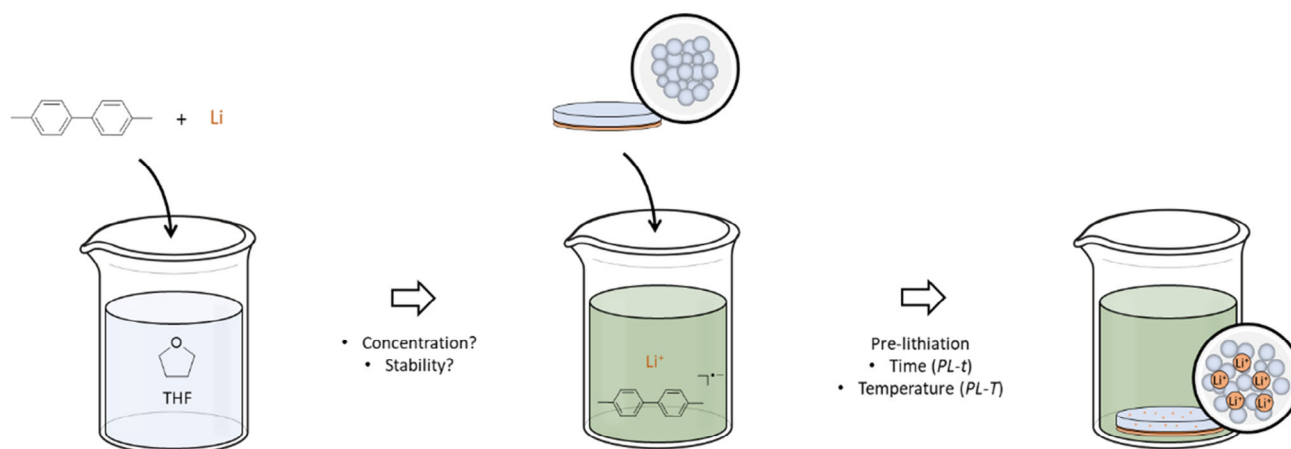


Figure 11. Schematic overview of the experimental prelithiation approach of Si-based anodes via LAC solution.

added and the solution was rigorously stirred for 30 min. The prepared solution was withdrawn (without Li metal) and the electrode added with a Li:active mass (AM) ratio of 5:1. The applied temperature and time for prelithiation are mentioned in the respective passage of the experiment.

Characterization: All extractions were done with acrylate fibers in headspace mode for 600 s. The sample was held at room temperature to prevent further aging by ongoing thermal decomposition during the sampling procedure. The SPME setup from CTC Analytics (Zwingen, Switzerland) controlled by the cycle composer software of the AOC 5000 autosampler (Shimadzu, Kyoto, Japan) was used. GC–MS experiments were executed on a Shimadzu GCMS-QP2010 Ultra with assembled AOC-5000 Plus autosampler and a nonpolar Supelco SLB-5 ms (30 m × 0.25 mm, 0.25 μm; Sigma Aldrich Chemie GmbH, Steinheim, Germany) column. Further parameters and sample preparation conditions were applied according to Horsthemke et al.^[45]

FT-IR was carried out to investigate the difference of the binder systems before and after being in contact to the LAC solution. The measurements were performed in a Vertex 70 spectrometer from Bruker-Optics using a KBr beam splitter, MIR light source and a deuterated L-alanine-doped triglycine sulfate detector with a scan velocity of 10 kHz and a KBr window. The obtained spectra were averaged over 64 scans with an optical resolution of 2 cm^{−1} in a frequency range between 500 and 4000 cm^{−1}. Before each measurement, a reference spectrum of an Ar-filled glovebox was measured to minimize the interferences of contaminated species.

XRD measurements of pre-lithiated SiNP800/KS4 and SiNW/Gr-electrodes were carried out using a Bruker D8 Advance X-Ray diffractometer with Ni-filtered Cu-Kα radiation (λ = 0.154 nm). The spectra were measured in a 2θ range from 10°–40° and 10°–60° with a respective step size of ≈0.04° and a step time of 1.8 s. A total number of 737 steps (≈22.1 min./scan) was carried out for the measurements between 10° and 40° with a rest step at the end to get a total measurement time of 25 min per scan. A total of 1229 steps (≈36.9 min./Scan) was done for the measurement between 10° and 60°. The diffractogram was referenced to the Beryllium reflection obtained by the measurement from 10 to 60°.

⁷Li MAS-NMR measurements were conducted at a 4.7 T Bruker Avance III spectrometer with a Larmor frequency of 77.9 MHz for ⁷Li. A commercially available Bruker double-resonance probe with 4 mm MAS rotors spinning at 10 kHz was used. All spectra were recorded with a pulse length of 4.5 μs (90° pulse), averaging 256 scans with relaxation delays of 4 s for Li_xC₆. The rotors were packed in an argon-filled glovebox and before packing the material was mixed with potassium bromide (KBr) to prevent frictional heating.

SEM measurements at an acceleration voltage of 3 kV of the NEs after first delithiation were performed using a Zeiss Auriga scanning electron microscope (Carl Zeiss). All electrodes were washed with 100 μL of dimethyl carbonate (DMC) prior to measurement to remove residual salts

and were transferred to the device via a shuttle to exclude unwanted reactions with air under reduced pressure.

Supporting Information

Supporting Information is available from the Wiley Online Library or from the author.

Acknowledgements

The authors thank the European Union for funding this work in the project 'SeNSE': This project received funding from the European Union's Horizon 2020 research and innovation program under grant agreement no. 875548. As partners in the project 'SeNSE', the authors thank ENWIRES for the supply of SiNW/Gr anode AMs.

Conflict of Interest

The authors declare no conflict of interest.

Data Availability Statement

The data that support the findings of this study are available from the corresponding author upon reasonable request.

Keywords

capacity excesses, Li inventories, lithium and capacity losses, lithium arene complexes, silicon-based anodes

Received: August 28, 2023

Revised: October 31, 2023

Published online: November 28, 2023

- [1] J. Kasnatscheew, R. Wagner, M. Winter, I. Cekic-Laskovic, *Top. Curr. Chem. Z* **2018**, 376, 16.
- [2] M. Winter, J. O. Besenhard, M. E. Spahr, P. Novák, *Adv. Mater.* **1998**, 10, 725.
- [3] N. Nitta, F. Wu, J. T. Lee, G. Yushin, *Mater. Today* **2015**, 18, 252.

- [4] T. Placke, G. G. Eshetu, M. Winter, E. Figgemeier, in *Lithium-Ion Batteries Enabled By Silicon Anodes* (Eds: C. Ban, K. Xu), Institution of Engineering and Technology, London **2021**, pp. 349–404.
- [5] D. Larcher, S. Beattie, M. Morcrette, K. Edström, J.-C. Jumas, J.-M. Tarascon, *J. Mater. Chem.* **2007**, *17*, 3759.
- [6] W.-J. Zhang, *J. Power Sources* **2011**, *196*, 13.
- [7] M. N. Obrovac, V. L. Chevrier, *Chem. Rev.* **2014**, *114*, 11444.
- [8] D. R. Gallus, R. Wagner, S. Wiemers-Meyer, M. Winter, I. Cekic-Laskovic, *Electrochim. Acta* **2015**, *184*, 410.
- [9] M. N. Obrovac, L. J. Krause, *J. Electrochem. Soc.* **2007**, *154*, A103.
- [10] F. Holtstiege, A. Wilken, M. Winter, T. Placke, *Phys. Chem. Chem. Phys.* **2017**, *19*, 25905.
- [11] F. Holtstiege, P. Bärnmann, R. Nölle, M. Winter, T. Placke, *Batteries* **2018**, *4*, 4.
- [12] N. Liu, L. Hu, M. T. McDowell, A. Jackson, Y. Cui, *ACS Nano* **2011**, *5*, 6487.
- [13] R. W. Grant, M. Sweetland, A. M. Acharige, US 9,598,789 B2, **2017**.
- [14] R. W. Grant, M. Sweetland, A. M. Acharige, US 10,128,487 B2, **2018**.
- [15] H. J. Kim, S. Choi, S. J. Lee, M. W. Seo, J. G. Lee, E. Deniz, Y. J. Lee, E. K. Kim, J. W. Choi, *Nano Lett.* **2015**, *16*, 282.
- [16] M. W. Forney, M. J. Ganter, J. W. Staub, R. D. Ridgley, B. J. Landi, *Nano Lett.* **2013**, *13*, 4158.
- [17] A. Shellikeri, V. G. Watson, D. L. Adams, E. E. Kalu, J. A. Read, T. R. Jow, J. P. Zheng, *ECS Trans.* **2017**, *77*, 293.
- [18] G. Wang, F. Li, D. Liu, D. Zheng, Y. Luo, D. Qu, T. Ding, D. Qu, *ACS Appl. Mater. Interfaces* **2019**, *11*, 8699.
- [19] T. Tabuchi, H. Yasuda, M. Yamachi, *J. Power Sources* **2005**, *146*, 507.
- [20] X. Zhang, H. Qu, W. Ji, D. Zheng, T. Ding, C. Abegglen, D. Qiu, D. Qu, *ACS Appl. Mater. Interfaces* **2020**, *12*, 11589.
- [21] J. Jang, I. Kang, J. Choi, H. Jeong, K.-W. Yi, J. Hong, M. Lee, *Angew. Chem.* **2020**, *132*, 14581.
- [22] R. Wang, H. Li, Y. Wu, H. Li, B. Zhong, Y. Sun, Z. Wu, X. Guo, *Adv. Mater.* **2022**, *12*, 2202342.
- [23] Y. Shen, J. Zhang, Y. Pu, H. Wang, B. Wang, J. Qian, Y. Cao, F. Zhong, X. Ai, H. Yang, *ACS Energy Lett.* **2019**, *4*, 1717.
- [24] Y. Shen, J. Qian, H. Yang, F. Zhong, X. Ai, *Small* **2020**, *16*, 1907602.
- [25] Y. Shen, X. Shen, M. Yang, J. Qian, Y. Cao, H. Yang, Y. Luo, X. Ai, *Adv. Funct. Mater.* **2021**, *31*, 2101181.
- [26] J.-S. Woo, H.-W. Lee, J.-H. Lee, S.-H. Han, W.-J. Kwak, *Mater. Today Energy* **2022**, *30*, 101156.
- [27] H. L. Cohen, G. F. Wright, *J. Org. Chem.* **1953**, *18*, 432.
- [28] K. Maruyama, T. Katagiri, *J. Phys. Org. Chem.* **1989**, *2*, 205.
- [29] B. R. Cook, B. B. Wilkinson, C. C. Culross, S. M. Holmes, L. E. Martinez, *Energy Fuels* **1997**, *11*, 61.
- [30] Y.-S. Su, J.-K. Chang, *Batteries* **2022**, *8*, 99.
- [31] N. Hamzelui, G. G. Eshetu, E. Figgemeier, *J. Energy Storage* **2021**, *35*, 102098.
- [32] P. Bärnmann, M. Mohrhardt, J. E. Frerichs, M. Helling, A. Kolesnikov, S. Klabunde, S. Nowak, M. R. Hansen, M. Winter, T. Placke, *Adv. Energy Mater.* **2021**, *11*, 2100925.
- [33] C. Heubner, T. Liebmann, O. Lohrberg, S. Cangaz, S. Maletti, A. Michaelis, *Batteries Supercaps* **2022**, *5*, e202100182.
- [34] J. Moon, H. C. Lee, H. Jung, S. Wakita, S. Cho, J. Yoon, J. Lee, A. Ueda, B. Choi, S. Lee, K. Ito, Y. Kubo, A. C. Lim, J. G. Seo, J. Yoo, S. Lee, Y. Ham, W. Baek, Y.-G. Ryu, I. T. Han, *Nat. Commun.* **2021**, *12*, 2714.
- [35] J. Li, J. R. Dahn, *J. Electrochem. Soc.* **2007**, *154*, A156.
- [36] B. Key, R. Bhattacharyya, M. Morcrette, V. Seznéc, J.-M. Tarascon, C. P. Grey, *J. Am. Chem. Soc.* **2009**, *131*, 9239.
- [37] G. W. Canters, E. de Boer, *Mol. Phys.* **1973**, *26*, 1185.
- [38] J. Kasnatscheew, T. Placke, B. Streipert, S. Rothermel, R. Wagner, P. Meister, I. C. Laskovic, M. Winter, *J. Electrochem. Soc.* **2017**, *164*, A2479.
- [39] J. Kasnatscheew, M. Evertz, B. Streipert, R. Wagner, R. Klöpsch, B. Vortmann, H. Hahn, S. Nowak, M. Amereller, A.-C. Gentschev, P. Lamp, M. Winter, *Phys. Chem. Chem. Phys.* **2016**, *18*, 3956.
- [40] J. Kasnatscheew, M. Börner, B. Streipert, P. Meister, R. Wagner, I. Cekic Laskovic, M. Winter, *J. Power Sources* **2017**, *362*, 278.
- [41] T. Dagger, J. Kasnatscheew, B. Vortmann-Westhoven, T. Schwieters, S. Nowak, M. Winter, F. M. Schappacher, *J. Power Sources* **2018**, *396*, 519.
- [42] V. L. Chevrier, L. Liu, R. Wohl, A. Chandrasoma, J. A. Vega, K. W. Eberman, P. Stegmaier, E. Figgemeier, *J. Electrochem. Soc.* **2018**, *165*, A1129.
- [43] P. Bärnmann, M. Diehl, L. Göbel, M. Ruttart, S. Nowak, M. Winter, T. Placke, *J. Power Sources* **2020**, *464*, 228224.
- [44] S. Karuppiyah, C. Keller, P. Kumar, P.-H. Jouneau, D. Aldakov, J.-B. Ducros, G. Lapertot, P. Chenevier, C. Haon, *ACS Nano* **2020**, *14*, 12006.
- [45] F. Horsthemke, A. Friesen, X. Mönnighoff, Y. P. Stenzel, M. Grützeke, J. T. Andersson, M. Winter, S. Nowak, *RSC Adv.* **2017**, *7*, 46989.